COMPUTER METHODS IN MATERIALS SCIENCE

2024, vol. 24, no. 2, 39–48
https://www.cmms.agh.edu.pl/2024_2_0838

An analytical model for the tool center point placement in Robotic Roller Forming

Thomas Stewens[1,2], Yi Liu[1], Ling Wang[3], Junying Min[1,*]

[1] School of Mechanical Engineering, Tongji University, Shanghai 201804, China.
[2] Technical University of Darmstadt, Darmstadt, Germany.
[3] Siemens DISW, Shanghai, China.

Abstract

Robotic Roller Forming (RRF) is a novel process using an articulated robotic manipulator that can bend Ultra-High Strength materials into thin-walled profiles. For high strength or difficult-to-form sheet materials, a laser can be employed to synchronously heat and soften the local material during RRF. The aim of RRF is to establish itself as a highly flexible process for rapid prototyping as well as for small batch production. However, in finished parts formed with different materials, a new defect that shapes the profile like that of a hook was observed. To overcome this defect and to improve the adaptability of the process, a new analytical model is suggested for the automatic calculation of the tool center point based on the given process parameters. The model was compared to the previous state, where the hook defect was noticeably reduced. Additionally, the control of the bend radius was studied, and the resulting bend radius diverged from the target radius by 0.04 mm (2.45%). Further, when examining the reproducibility, the same bend angles could be achieved as in previous experiments using the constant laser power density. Finally, the development of the bend allowance was studied in various experiments. The analytical model for RRF is a promising method for calculating tool placement and controlling the bend radius in a freeform environment.

Keywords: robotic forming, bending, analytical model, tool center point

1. Introduction

In recent years, lean principles have become the standard for modern manufacturing. The focus herein lies on reducing waste and manufacturing based on a pull system (Womack & Jones, 1996). To satisfy lean principles and customer-oriented production, new highly adaptable manufacturing methods must be developed. Therefore, flexible, adaptable processes capable of rapid prototyping are being developed to satisfy the needs of modern manufacturing processes.

To satisfy the requirements of personalized production of parts, robots are gaining recognition for their flexibility, and new processes have been developed. This includes Incremental Sheet Forming (ISF), which is a highly adaptable process but struggles with the accuracy due to the low stiffness of the robot manipulator and the springback of the sheet metal, therefore, an analytical model is used to estimate the process better (Barthi et al., 2024). Another study introduced a dynamic model using a digital twin to overcome and control the resisting forces (Petru et al., 2024). The use of robots for grasping and repositioning the workpiece was

* Corresponding author: junying.min@tongji.edu.cn
ORCID ID's: 0009-0005-6887-3267 (T. Stewens), 0000-0003-4980-7916 (Y. Liu), 0009-0001-8233-3671 (L. Wang), 0000-0002-1754-6259 (J. Min)

verified for the press brake (Aomura & Koguchi, 2002). Another instance in the application of robots for easing the forming process is Mechatroforming® or robotic hammer forming which avoids the need for manual labor and overcomes the cost of such labor and lack of experts for this skill using a robot to adjust the metal sheet in the hammering unit (Ilangovan et al., 2016).

Generally, forming is a process where the specimen experiences a permanent change in shape without any significant alteration in its mass or cohesiveness (DIN, 2020). Bending is divided into two subgroups, the first being the tool having a linear trajectory or a rotational movement of the tool (DIN, 2003). A special form is freeform bending. The requirement of freeform bending is that the tool merely passes the bending forces onto the workpiece, and the radius of the tooltip, or the bend support must be smaller than the final radius of the workpiece (Doege & Behrens, 2017). This type of forming is used in swivel bending where the bend radius is controlled via the placement of the tool (Klocke, 2006). Further, bending processes underly certain phenomena that increase the difficulty of setting up the process, such as springback and the shift of the neutral axis.

Generally, the neutral layer remains at the same length but shifts towards the inner side of the bend. When the ratio of the bending radius to the thickness becomes too small, the workpiece starts to develop cracks in the bending area. Therefore, minimal bend radii are defined for the materials. The *k*-factor is introduced to describe the shift of the neutral layer and is defined as the ratio of the neutral layer position to the thickness of the workpiece. The ideal *k*-factor where no shift occurs is 0.5. The *k*-factor is not only influenced by the bend radius to thickness ratio but also by the process being used and the material properties (Oberg et al., 2020). During the bending process, the elastic deformation within the specimen aims to return to a state of equilibrium in terms of inner stress after removing the external force. As a result, the specimen reverts to the original state to a certain extent until this state of equilibrium is achieved (Fritz & Günter, 2015). This defect or phenomenon is commonly referred to as springback. Decreasing the sheet thickness and increasing the bend angle, consequently, increases springback. Increasing the elastic modulus and strain hardening, as well as decreasing the bend radius, lead to a decrease in springback (Cinar et al., 2021). The relationship between the ratio of the springback radius to the initial radius and the ratio of the springback radius to the thickness of the sheet is nearly linear and material-independent (Panthi et al., 2007). It is also found that controlling the forming load can improve the effect of springback (Panthi et al., 2010). Springback cannot be generalized across all materials and even differs between various processes (Badr et al., 2017). This, in turn, means that the neutral axis and springback should be regarded in the setup and development of new processes.

One such process is Robotic Roller Forming (RRF), introduced by Liu et al. (2021) as a novel forming process to combine the benefits of robots and roller forming and expanded this process to Laser-assisted Robotic Roller Forming (LRRF). The strength of this process follows the trend of small batch and flexible production being in growing demand (Allwood et al., 2016). Figure 1 shows the Laser-assisted Robotic Roller Forming cell and the schematic view of a three-pass process for LRRF. A laser pre-heats the metal sheet locally, and is then formed by a roller attached to a robot manipulator. The toolpath of LRRF can be understood as a combination of a rotational tool path for the positioning and a linear trajectory during the bending depicted in Figure 1. The rotational part of the LRRF toolpath is conceptionally identical to that of swivel bending. The current conventional method to setup the LRRF process is done manually. This means the operator has to set up at least two positions for each pass for the setup. This results in 16 positions having to be prepared for an 8 pass process. If any of the process parameters are changed, such as the sheet thickness, the bend angle increment or the number of passes, the setup process has to be repeated.

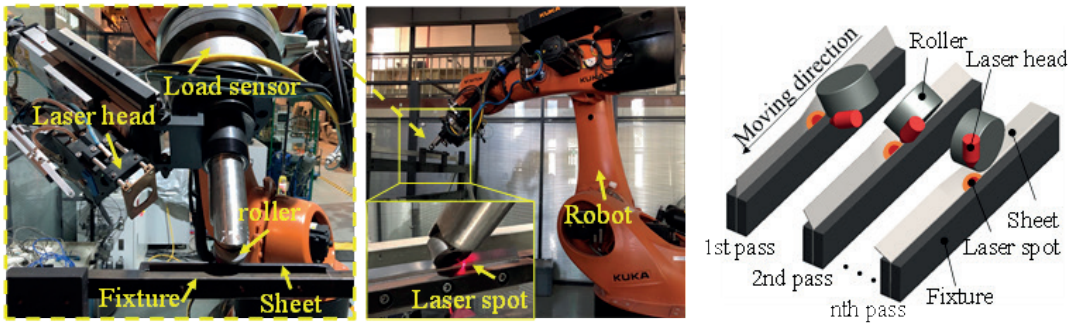

Fig. 1. LRRF cell and schematic view of Laser-assisted Robotic Roller Forming (Min et al., 2023)

The LRRF process has been proven to be capable of enhancing the bending performance of high-strength thin-walled structures once the forming defects are solved (Liu et al., 2023a). One of the main defects that occurs in specimens formed via LRRF is edge waves. To decrease the edge wave defects, the forming parameters were adapted. To further decrease the defects, laser power is introduced, as seen in Figure 1, which heats the area right before the forming roller. As a result, the forming forces decreased by 20%, removing the edge wave defect with higher geometrical accuracy and fewer passes (Liu et al., 2021). In high-strength materials, such as MS1300, the addition of laser heating not only decreases the edge waves but also increases the ductility of the workpiece during bending, leading to longitudinal cracks and microcracks being removed (Liu et al., 2022). A simulation was run to approximate what the microstructure would be like during the laser-assisted robotic rolling forming (LRRF) process using thermo-metallurgical-mechanical modeling (Liu et al., 2023b). To optimize the parameters, Min et al. (2023) introduced the constant laser power density, finding that increasing the laser power density leads to a smaller bend radius. The optimal value for the laser power density was found at 10 J/mm^2, yielding a springback of 0.8° with a bend radius-to-thickness ratio of ~1.2. Additionally, during the experiments, the decrease in force was attributed to the decreased yield strength of the material and the deformation taking place before the formation of new martensite.

Parameters such as the length or thickness of the workpiece both need the program to be set up entirely new as well. Further, the positioning of the roller depends on what the current practitioner adapting the process deems sufficient accuracy. Therefore, reproducing the same program in a different robotic cell cannot be done. As a result, comparing results can only be effectively done if the same cell is using the same robotic program. Another issue that arises can be seen in Figure 2. The hook defect that occurs in the bending area around the clamped section happens because the workpiece is pressed down directly to the surface of the fixture. The workpiece, due to the pressing, cannot slip in the direction of the flange, and the material yields in the bend region, which mimics the achievement of a smaller bend radius.

This research in this paper aims to generate an easy to apply analytical model for the placement of the TCP for LRRF to standardize and decrease the setup time of the LRRF process with new process parameters. This model can be extended and used on the positioning of the roller in adaptive or flexible roll forming applications such as flexible roll forming (FRF), 3D roll forming, or flexible re-configurable roll forming (FRRF) (Abeyrathna et al., 2016; Ghiabakloo et al., 2018; Sedlmaier et al., 2017). The analytical model is presented and experiments to validate the model and its applicability in comparison to the conventional process setup are carried out and the results regarding the general and process specific defects and the process forces are analyzed. Further, the repeatability using a constant laser power density of 10 J/mm^2 was tested. Finally, the results are discussed and a verdict on the effectiveness and applicability is given.

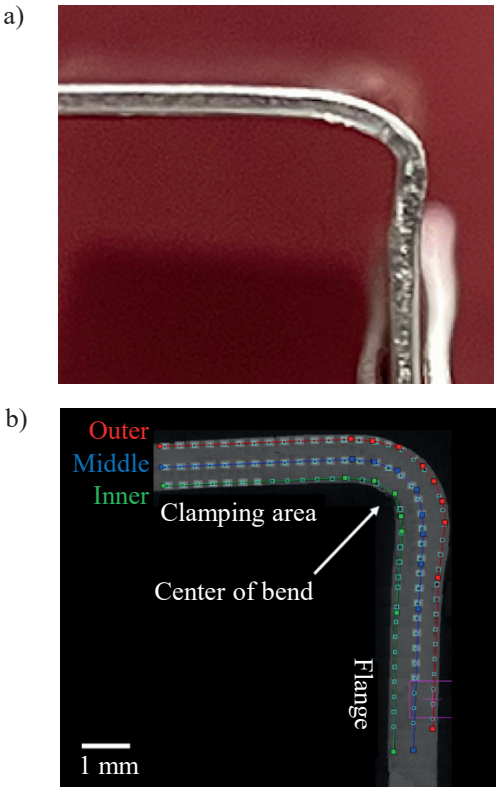

Fig. 2. Hook defect during bending: a) leading bend edge of conventionally bent A6061 specimen with RRF; b) cross-section of MS1300 workpiece bent with LRRF (Liu et al., 2022)

2. TCP-placement calculation

To unlock the potential of LRRF the placement of the tool is overhauled to be independent of the tool geometry and to be calculated via using the process parameters. For the calculation of the TCP, the cross-section of the workpiece is observed, as shown in Figure 3. The workpiece is split into three sections: the clamped section, the bend section, and the flange. The bending is assumed to occur in the bend section and is equal to the length of the bend allowance l_{bend}. Further, the bend is idealized with the neutral axis,

red dashed line in Figure 3, remaining in the middle and the bend exhibiting uniform behavior. Using the target bend angle α_t and the target bend radius r_t, the bend allowance is calculated from the neutral axis with the workpiece thickness t:

$$l_{\text{bend}}(\alpha_t, r_t, t) = \frac{\alpha_t}{360°} 2\pi \left(r_t + \frac{t}{2} \right) \tag{1}$$

With the bend allowance remaining constant throughout the bending process, the length of the bend section and the length of the flange are established.

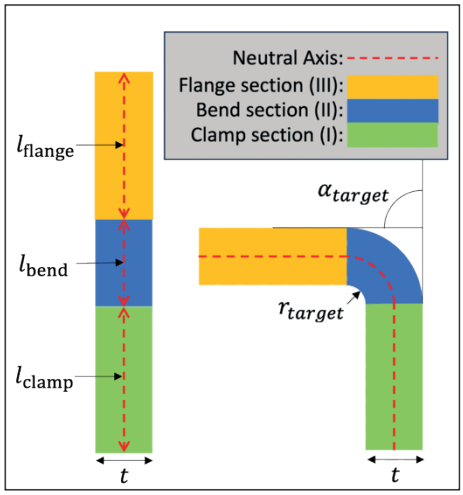

Fig. 3. Cross-sectional view of the workpiece: left – unbent workpiece, right – final form of workpiece

Next, the placement of the TCP for the incremental process is calculated. The geometric relationship is set up using the process parameters as input variables to calculate the position. For this, the bend angle of the increment α_{bend} and the bend allowance l_{bend} are needed. Figure 4 shows the geometric relations. First, the cartesian coordinate system with the origin in $\vec{O}$ is used to calculate the coordinates:

$$\vec{x}_{b,e} = \frac{180° \cdot l_{bend}}{\pi \alpha_{bend}} \begin{pmatrix} 1 - \cos(\alpha_{bend}) \\ \sin(\alpha_{bend}) \end{pmatrix} \tag{2}$$

where the flange and the bend section intersect. Next, the tangent to the circle spanned by the bend section is used to align the tool center point at a distance d to $\vec{x}_{b,e}$ to calculate the conceptional placement of the TCP in the neutral axis:

$$\vec{x}_{TCP,nl} = \vec{x}_{b,e} + d \cdot \vec{m}_{n,tan} \tag{3}$$

Finally, the orthogonal of the tangent is used to calculate the placement of the TCP.

$$\vec{x}_{TCP} = \vec{x}_{TCP,nl} + 0.5t \cdot \vec{m}_{n,sec} \tag{4}$$

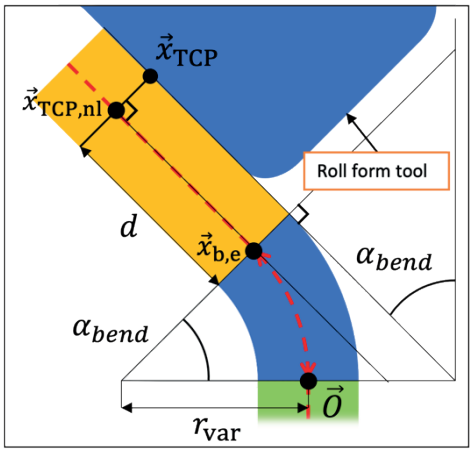

Fig. 4. Visualization of calculating the TCP touch point $\vec{x}_{\text{TCP}}$ of the workpiece

3. Experimental setup

This section further elucidates the equipment that is used for the research. The KUKA KR600 R2830 is a six-axis heavy-duty robot. The maximum range is 2826 mm, with a position repeatability of 0.08 mm. The nominal load capacity is 600 kg. The control system used is the KUKA KR C4. The load sensor is the OMEGA191 of ATI Industrial Automation, Apex, and the forces were captured at a rate of 50 Hz during the experiments with a resolution of 0.75 N for F_z and 0.375 N for both F_x and F_y (ATI Industrial Automation, 2024). The laser used is an MFSC 4000 W fiber laser. The laser is equipped with the ZF-HH003A head model and a 4 mm × 2 mm rectangular laser spot, with the short side aligned with the direction of movement of the robot. The forming roller used on the master robot is a cylindrical forming roller with a 50 mm diameter and a 25 mm width. The workpiece was clamped between two bars and fixed with two M8 screws. The rectangular bar of the fixture that the workpiece was bent over has a 1 mm radius. The analysis was done using the digital inclinometer for the bending angle of the parts, with a resolution of 0.05° and an accuracy of 0.2°. The thickness and dimensions of the sheets were measured with an electronic caliper at a resolution of 0.01 mm.

Next are the materials that were used for the experiments. The steel that was used is the quenched and portioned steel QP1180 from BAOsteels. The aluminum alloy is A6061-T6. The materials were selected due to the trend of the automotive industry towards lightweight and high-strength materials. For QP1180, test strips of the experiment batch were supplied, with which the mechanical properties of the material were analyzed to ensure their quality. The mechanical properties of A6061-T6 were

gathered from secondary sources. Table 1 shows the results of the tensile test for the various materials.

Table 1. Mechanical properties of materials

Materials	QP1180	A6061-T6*
Elastic modulus [GPa]	199.5	68.9
Total elongation [%]	15	10
Yield strength [MPa]	915	276
Tensile strength [MPa]	1252	310

* data from MakeItFrom.com (2020)

For the three experiments, each specimen was cut into a rectangular metal sheet. An example, illustrated in Figure 5, shows the nominal height of 50 mm and the nominal length of 100 mm. The same setup was used for each experiment, using a clamp to fix the specimen to the workbench. Each experiment was done using a number of 6 passes. Further, unless specified otherwise, the scanning speed was set to 30 mm/s, and the target bend radius was an inner radius of 1 mm.

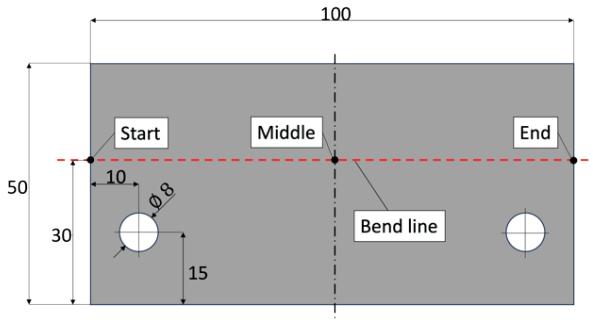

Fig. 5. Example metal sheet for Robotic Roller Forming

3.1. AM-experiment

The purpose of the analytical model validation experiment (AM-experiment) is to test the feasibility of the analytical model in the real process. For this, a blank robotic program is set up where the TCP is placed at the origin x and y coordinates while the z coordinates are fixed to the beginning and end of the specimen length. The positioning of the TCP is then calculated using the analytical model and superimposed on the blank robotic program positions. The specimen used for this experiment is the A6061-T aluminum alloy without the Laser (laser power equal to zero watts). The conventional method was compared with the analytical model. The conventional method experiment is referred to as CM, and the analytical model experiment as AM.

3.2. BR-experiment

In the bend radius experiment (BR-experiment), the concept of adapting the bend radius based on the mathematical model is evaluated. This is done to obtain insights into the bending behavior of the materials and the dominating factors of the bend radius. Further, the influence of the laser heating on the bend radius is studied. The materials used for this experiment are QP1180 and A6061. The QP1180 steel was selected to represent the high-strength materials that need laser heating at 1200 W to decrease the load on the robot. The aluminum alloy A6061 was selected to study the behavior of the bend radius in a uniform material environment. The configuration is shown in Table 2. The target radii of the mathematical model were set to 1 mm, 3 mm, and 5 mm.

Table 2. BR-experiment with QP1180 and A6061

Shorthand reference	BR_QP_1A BR_QP_1B	BR_QP_3A BR_QP_3B	BR_QP_5A BR_QP_5B	BR_AL_1	BR_AL_3	BR_AL_5
Material	–	QP1180	–	–	A6061	–
Laser power [W]	–	1200	–	–	0	–
Target bend radius [mm]	1	3	5	1	3	5

3.3. CD-experiment

The constant laser power density experiment (CD-experiment) is an extension of the model validation using the mathematical model for the analysis of constant laser power as an indicator of constant quality. The concept is based on a previous study to further understand LRRF and produce parts of similar quality under varying process parameters. Further, the repeatability of the analytical model is being investigated. The material used for this experiment is QP1180, and the configurations are shown in Table 3.

Table 3. CD-experiment

	CD_1 & CD_2	CD_3 & CD_4
Scanning speed [mm/s]	30	22.5
Laser power [W]	1200	900

4. Results

The results are subcategorized into different experiments: the AM-experiment with the aim of comparing the results from the analytical model to the conventional method, the CD-experiment which highlights the repeatability and reproducibility, and finally the BR-experiment which investigates the ability to control the bend radius via the tool placement.

4.1. Validation of analytical model

The analytical model for the TCP placement was applied to the robotic program and the analytical forming method (AM) was compared with the conventional forming method (CM). Figure 6 are the cross-sections of the two profiles. The hook defect, which is the buckling of the profile against the bending direction, can be observed as well. CM exhibited a more pronounced hook effect compared to AM.

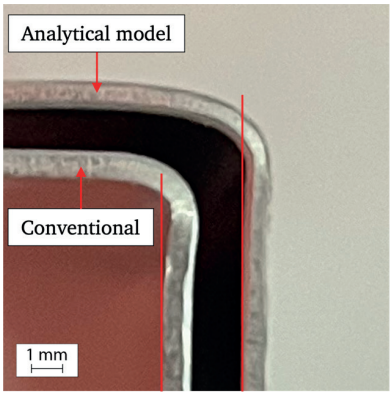

Fig. 6. Comparison of hook effect between a conventionally formed profile and an analytically model formed profile

The leading edge of the profiles exhibits an overbending of 2° for AM and 2.4° for CM past the target of 90°. The bending angle of the trailing edge is down to 86.6° (AM) and 86.8° (CM). However, this decrease is not linear, as Edge waves can be examined across the entirety of both profiles. The bend radius for both workpieces shows a different trend. While AM has an average outer bend radius of 2.96 mm (±0.3 mm), the outer bend radius of the CM part is 2.63 mm.

Figure 7 shows the comparison of the process forces using the conventional method and the analytical method. During the first pass, the peak of the process forces of the analytical forming method exceeds the conventional method by 15.8 N. However, for the rest of the passes, the bending force of CM exceeds that of AM. CM has a minimum peak at 227.1 N during the first pass and a maximum during the final pass at 375.1 N, averaging 313.6 N across all six passes. On the other hand, AM has its lowest peak in the second pass at 198.9 N and the highest force during the fourth pass at 276.3 N. The average peak force for the analytical method is 233.3 N. The standard deviation of AM is 25.6 N less than half of the conventional forming at 58.4 N.

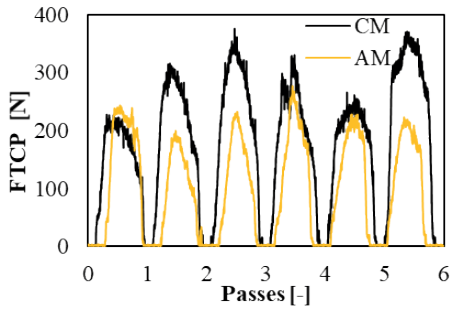

Fig. 7. Comparison of the process forces for the conventional and the analytical part

4.2. Repeatability of LRRF

Figure 8 illustrates the repeatability in the form of the normal distribution of the bending force at the TCP for the 1200 W and 30 mm/s experiment with CD_1 and CD_2, as well as for CD_3 and CD_4 at 900 W and 22.5 mm/s. The difference in standard deviation for 1200 W and 30 mm/s is 2.25 N. For the 900 W and 22.5 mm/s experiments, the difference in the standard deviation is 9.11 N.

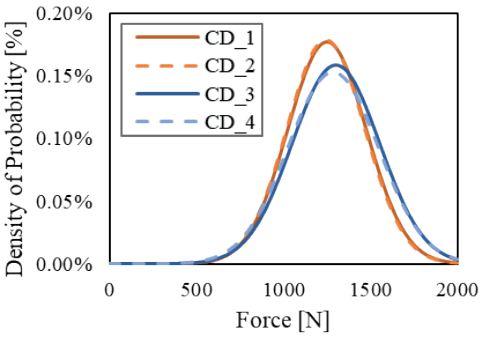

Fig. 8. Normal distribution of average peak force of LRRF for QP1180 of CD_1 to CD_4

Table 4 summarizes the differences between CD_1 and CD_2 in the first row for the 1200 W 30 mm/s experiments as well as for CD_3 and CD_4 in the 900 W and 22.5 mm/s experiments in the second. These results build on the previously observed insight that the process has high repeatability. This finding supports the decision to sustainably use the resources. The difference in both the bend angle and the bend radius is negligible for CD_1 and CD_2. Further, the forces only differed by 7.05 N.

Table 4. Differences of peak force, bend angle and bend radius for repeatability

	ΔF_{TCP} [N]	$\Delta\alpha_{bend}$ [°]	Δr_o [mm]
1200 W & 30 mm/s	7.05	0.250	0.07
900 W & 22.5 mm/s	15.84	0.083	0.21

4.3. Controlling the bending radius

The BR-experiment is divided into two sections the BR_AL series without the laser and the BR_QP series with the laser. For further information on the configuration of the experiment, refer to the experiment information in section 3. The uniform bending without the laser is analyzed first. Figure 9 shows the middle cross-section of the specimen as well as the profile for the bend radius of each specimen in an ascending order. For BR_1 and a target radius of 1 mm, the inner bend radius resulted in 1.83 mm. The cross-sectional profile shows no rounding in the flange. Next, the bend radius for BR_AL_3 is 3.38 mm on average, and a slight rounding of the flange is observed. Further, the bend radius in the starting section is slightly overbent. Finally, BR_AL_5 has a noticeable rounding of the flange and shows a similar behavior with the starting section being overbent. The average bend radius of the BR_AL_5 experiment is 5.08 mm. Across all three cross sections of the workpieces, a decrease in the flange length is observed with an increase in the bend radius.

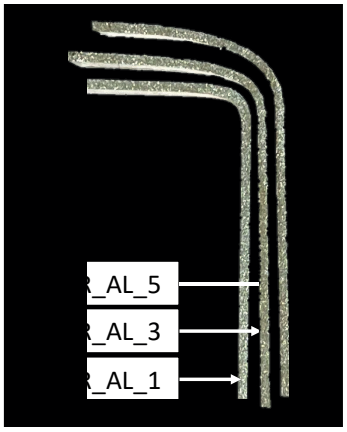

Fig. 9. Cross-section results for various bend radii of A6061 profiles

The measurements for the bending force are illustrated in Figure 10. During the BR_AL_1 experiment, an average bending force of 233.3 N was measured. The peak was at 276.3 N in the fourth pass. The standard deviation of the results is 10.97%. For the BR_AL_3, with the increased target bending radius, the average force decreased to 169.8 N with a standard deviation of 4.81%. Further, BR_AL_3 peaks at 183.0 N during the final pass. Like BR_1, BR_AL_5 peaks at 168.5 N on the fourth pass. The average for BR_AL_5 is 156.3 N, with a standard deviation of 10.12%. The process forces of BR_AL_1 are greater than those of BR_AL_3. In total, BR_AL_5 has the lowest force. However, during the fifth path, the peak force of BR_AL_5 is virtually equal to that of BR_AL_3.

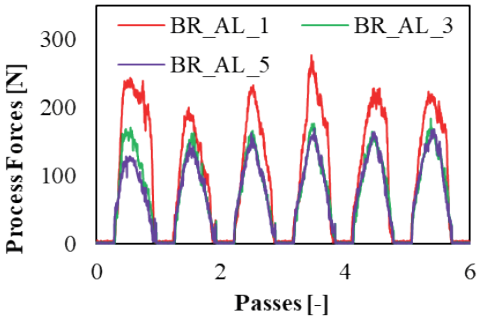

Fig. 10. Process forces of the bend radius experiment (BR) for A6061-T6

The results of the bend radius experiment with laser assistance are shown below in Figure 11. The clamped leg of each specimen is aligned to emphasize the location of the beginning of the bend. The beginning of the bend is measured from the bottom of the clamped leg. The bend for BR_QP_1A begins at 30.5 mm (refer to the red dashed line). As the bend radius is increased to 3 mm and 5 mm the location of the bend also shifts along the metal sheet. Further, only the inner radius r_i for BR_QP_1A of 1.83 mm and BR_QP_1B of 1.67 mm is evaluated. The reason is that the quality of the geometry is subpar for the other experiments due to the irregular shape that is observed in the bend region of the flange. This is a new defect that has not been observed before. However, the average outer bend radius r_o for BR_QP_3A, BR_QP_3B, BR_QP_5A all shared the same result of 2.42 mm and for BR_QP_5B it is 2.5 mm.

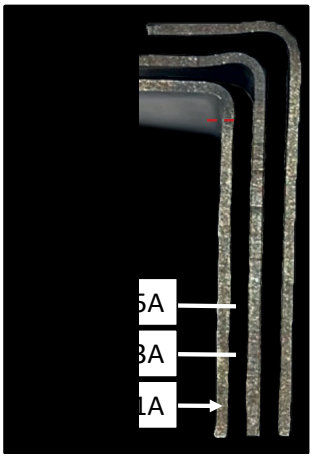

Fig. 11. Cross-section results for the bend radius experiment for QP1180 formed by Laser-assisted Robotic Roller Forming

5. Discussion

The goal of the analytical model was to establish a method to calculate the placement of the tool center point of the robot. This model is used to set up new robotic programs for LRRF utilizing the process parameters. Further, the model aims to reduce the hook defect that occurs during the forming process and test whether the bend radius could be controlled with the placement of the TCP. The model is compared to the conventional forming for evaluation. Further, the reproducibility of results and the control of the bend radius are tested.

Introducing the model shows a reduction of the hook effect. In line with the hypothesis, the geometric defect is induced by the metal being pressed down to the fixture, and the surplus of bend allowance breaks away in the hook defect. To overcome this, the analytical model allocates the minimum necessary bend allowance for the specimen to bend around.

As seen in Figure 12, not only is the average bending force of the analytical model experiment significantly lower, but also the average peak force is less scattered compared to the conventional method. The outer bend radius results show that the average increased by 0.33 mm. Contrary to the expected outside radius of 2 mm for the analytical model, it is nearly 3 mm. The inner radius of 1.83 mm also exceeds the expected bend radius of 1 mm. These results should be considered when improving the placement of the TCP. One reason for this could be the accuracy of the reference point and the setup of the reference coordinate system in the robot system. This is further explored in the discussion of the BR-experiment. Another reason is that the bend radius of CM is decreased due to the hook effect. Also, as Liu et al. (2024) pointed out, the target radius is difficult to achieve due to the stiffness deformation of the robot leading to the deviation of the tool trajectory, especially for a small bending radius. The bend angle results are illustrated; the springback increased by 0.5°. During the process, the total peak force is reduced by 26.3%, and the average force peak is reduced by 25.6%. The deviation of the process is also reduced by 56.1%. In line with the hypothesis to decrease the hook effect, this also leads to the process not having to waste force pressing directly onto the fixture. While the increased force for CM can partially be attributed to the large bend radius the same cannot be said for the force distribution. The force distribution improved, this suggests that the lever arm is controlled better during AM leading to a more uniform force distribution during the process. Aside from the repeatability, the reproducibility of previous studies is also compared. For this, a constant laser power density of 10 J/mm^2 using 1200 W and 30 mm/s is used. A springback angle of 0.8° was achieved in previous experiments (Min et al., 2023). With the same configuration, the CD-experiment achieved a springback angle of 0.8° as well.

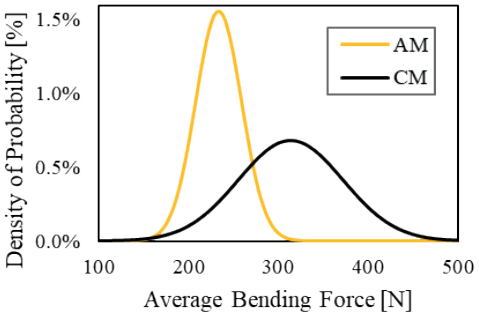

Fig. 12. Summary of AM-Experiment for AM (analytical) and CM (conventional): process force distribution

Figure 13 summarizes the results of the BR-experiment. In the graph, the results of the BR_AL experiment series indicate that increasing the bend radius decreased the process forces for the bending process. The data suggest that the decrease in process forces is not linear. However, the non-linearity can also be attributed to the length of the flange being limited, and as a result, the length of the lever arm to bend is decreased when the bend radius increases. Further, the results of the inner bend radii support the theory that the bend radius can be controlled with the placement of the TCP, similar to the concept of controlling the bend radius used in swivel bending (Klocke, 2006). Further, the data also shows that with the increase in bend radius, the variability of the bend radius across the profile also increased. It should be noted that the fixture has a rounding with a radius of approximately 1 mm. This rounding influenced the length of the allocated bend allowance. When adding the additional millimeter to the bend allowance, the target radius of each setting is increased by 0.64 mm for each setting. Therefore, relatively speaking, the influence is biggest for the bend target of 1 mm in BR_AL_1, and the influence decreases when increasing the target bend radius. Disregarding the overbend due to the edge waves in the start section of the bend radii, the difference amounts to 0.3 mm for BR_AL_1, 0.11 mm for BR_AL_3, and 0.15 mm for BR_AL_5. The laser-assisted experiments showed very little overbending and edge waves. Here, the bend radius is 1,67 mm for BR_QP_1A and BR_QP_1B. When using high-strength materials, such as QP1180, laser assistance is used. During the BR-experiment with QP1180 and the laser, a new defect was discovered, which showed a hook defect on the flange (refer to Figure 11). The results also indicate that the bend allowance during LRRF is not only dictated by the placement of the TCP but also by the laser-spot size. The reason for the flange dipping is due to the robot pressing the flange down while the bend radius reaches

a natural minimum. This is supported by the fact that for both BR_QP_3A and BR_QP_5A, the same outer bend radius is measured. Further, the data also indicates that the location of the bend is controlled by the location of the laser, and the free-standing section of the sheet metal is not deformed. This is supported by the fact that an increased bend radius allocates more bend allowance, and the laser is currently fixed to a certain angle relative to the forming tool. As a result, increasing the allocated bend allowance shifts the laser up as well, leading to the heated area being higher. These findings shed new light on the challenges and opportunities that are faced when bending high-strength metal sheets, such as QP1180, using LRRF. On the one hand, the laser spot size corresponds to the maximal achievable bend radius, and therefore, a greater bend radius could not be achieved. On the other hand, the laser can control the height at which the bend starts without a supporting tool to a certain extent.

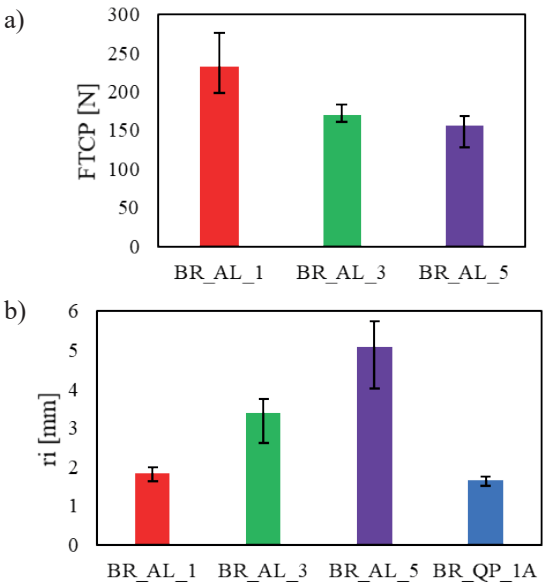

Fig. 13. Summary of BR-experiment:
a) average bending force; b) inner bend radius

The analytical model decreased the time to set up a new program and significantly reduced the hook-effect that is observed in conventional forming. The bending force is greatly reduced, and the bend radius can be controlled to a certain extent using the positioning of the TCP. Further, following the BR_QP experiments, it can be assumed that the maximum bend allowance and, therefore the bend radius are limited by the laser spot size. While larger radii cannot be produced for the LRRF, the position of the bend for sufficiently strong materials is dictated by the laser spot position.

6. Conclusion

In this paper, the method of calculating the analytical model is presented, and the method of implementing the analytical model follows suit. The applicability of the analytical model is established in the AM experiment; reproducibility and repeatability are studied in the CD experiment; and control of the bend radius is established in the BR experiment. The key takeaways are the reduction of the hook defect during RRF and LRRF, which reduces the average peak force by 25.6% and the deviation by 56.1%, leading to a more effective and balanced process. Further, the reproducibility of the analytical model is found to produce similar results to the previous experiments while also reducing the hook defect. For repeatability, negligible deviations as low as 7.05 N for the peak force, 0.25° for the bend angle, and 0.07 mm for the outer bend radius are found. Finally, the bend radius was able to be controlled, reaching deviations of the target bend radius as little as 2.45%. The control of the bend radius using LRRF brings forth a new hypothesis: that the location and size of the bend allowance are dictated by the laser spot.

References

Abeyrathna, B., Abvabi, A., Rolfe, B., Taube, R., & Weiss, M. (2016). Numerical analysis of the flexible roll forming of an automotive component from high strength steel. *IOP Conference Series: Materials Science and Engineering*, *159*, 5–12. https://doi.org/10.1088/1757-899X/159/1/012005.

Allwood, J. M., Duncan, S. R., Cao, J., Hirt, G., Groche, P., Kinsey, B., Kuboki, T., Liewald, M., Sterzing, A., & Tekkaya, A. E. (2016). Closed-loop control of product properties in metal forming. *CIRP Annals*, *65*(2), 573–596. https://doi.org/10.1016/j.cirp.2016.06.002.

Aomura, S., & Koguchi A. (2002). Optimized bending sequences of sheet metal bending by robot. *Robotics and Computer-Integrated Manufacturing*, *18*(1), 29–39. https://doi.org/10.1016/S0736-5845(01)00031-X.

ATI Industrial Automation – A Novanta Company (n.d.). *F/T Sensor: Omega191 IP65/IP68*. https://www.ati-ia.com/products/ft/ft_models.aspx?id=Omega191+IP65%2FIP68.

Badr, O. M., Rolfe, B., Zhang, P., & Weiss, M. (2017). Applying a new constitutive model to analyse the springback behaviour of titanium in bending and roll forming. *International Journal of Mechanical Sciences*, *128–129*, 389–400. https://doi.org/10.1016/j.ijmecsci.2017.05.025.

Bharti, S., Paul, E., Uthaman, A., Krishnaswamy, H., Klimchik, A., & Boby, R. A. (2024). Systematic analysis of geometric inaccuracy and its contributing factors in roboforming. *Scientific Reports*, *14*, 20291. https://doi.org/10.1038/s41598-024-70746-3.

Cinar, Z., Asmael, M., Zeeshan, Q., & Safaei, B. (2021). Effect of springback on A6061 sheet metal bending: A review. *Jurnal Kejuruteraan*, *33*(1), 13–26.

Doege, E., & Behrens, B.-A. (2017). *Handbuch Umformtechnik*. Springer.

DIN (2003). DIN 8586:2003-09: *Fertigungsverfahren Biegeumformen – Einordnung, Unterteilung, Begriffe*.

DIN (2020). DIN 8580:2020-1: *Fertigungsverfahren – Begriffe, Einteilung*.

Fritz, A. H. (2015). *Fertigungstechnik* (S. Günter, Ed.). Springer Vieweg Berlin, Heidelberg.

Ghiabakloo, H., Kim, J., & Kang, B.-S. (2018). An efficient finite element approach for shape prediction in flexibly-reconfigurable roll forming process. *International Journal of Mechanical Sciences*, *142–143*, 339–358. https://doi.org/10.1016/j.ijmecsci.2018.05.005.

Ilangovan, B., Monfared, R. P., & Jackson, M. (2016). An automated solution for fixtureless sheet metal forming. *The International Journal of Advanced Manufacturing Technology*, *82*, 315–326. http://doi.org/10.1007/s00170-015-7366-x.

Klocke, F. (2006). *Fertigungsverfahren* (vol. 4: *Umformen*). Springer Vieweg Berlin, Heidelberg.

Liu, Y., Min, J., & Lin, J. (2021). Robotic roller forming process and strategies to eliminate geometrical defect of edge waves. In G. Daehn, J. Cao, B. Kinsey, E. Tekkaya, A. Vivek, & Y. Yoshida (Eds.), *Forming the Future. Proceedings of the 13th International Conference on the Technology of Plasticity* (pp. 479–491). Springer Cham. https://doi.org/10.1007/978-3-030-75381-8_40.

Liu, Y., Min, J., Zhang, J., Cai, W., Carlson, B. E., Bobel, A. C., Hector Jr, L. G., & Sachdev, A. K. (2022). Laser-assisted robotic roller forming of an ultrahigh strength maternsitic steel. *Journal of Manufacturing Processes*, *82*, 109–202. https://doi.org/10.1016/j.jmapro.2022.07.066.

Liu, Y., Qiu, J., Wang, J., Bambach, M., & Min, J. (2023a). Fabrication of thin-walled hat-shaped beams from ultrahigh strength steel by laser-assisted robotic roller forming. *Smart Manufacturing*, *1*, 2340001. https://doi.org/10.1142/s273754982340001x.

Liu, Y., Wang, J., Cai, W., Carlson, B. E., Lian, J., & Min, J. (2023b). A thermo-metallurgical-mechanical model for microstructure evolution in laser-assisted robotic roller forming of ultrahigh strength martensitic steel. *Journal of Materials Research and Technology*, *25*, 451–464. https://doi.org/10.1016/j.jmrt.2023.05.228.

Liu, Y., Qiu, J., Wang, J., Lian, J., Hou, Z., & Min, J. (2024). An iterative path compensation method for double-sided robotic roller forming of compact thin-walled profiles. *Robotics and Computer-Integrated Manufacturing*, *86*, 102689. https://doi.org/10.1016/j.rcim.2023.102689.

MakeItFrom.com (2020). *6061-T6 Aluminum*. https://www.makeitfrom.com/material-properties/6061-T6-Aluminum.

Min, J., Wang, J., Lian, J., Liu, Y., & Hou, Z. (2023). Laser-assisted robotic roller forming of ultrahigh-strength steel QP1180 with high precision. *Materials*, *16*(3), 1026. https://doi.org/10.3390/ma16031026.

Oberg, E., Jones, F. D., Horton, H., Ryffel, H., & McCauley, C. (2020). *Machinery's Handbook* (L. Brengelman, Ed.). Industrial Press.

Panthi, S. K., Ramakrishnan, N., Pathak, K. K., & Chouhan, J. S. (2007). An analysis of springback in sheet metal bending using finite element method (FEM). *Journal of Materials Processing Technology*, *186*(1–3), 120–124. https://doi.org/10.1016/j.jmatprotec.2006.12.026.

Panthi, S. K., Ramakrishnan, N., Ahmed, M., Singh, S. S., & Goel, M. D. (2010). Finite Element Analysis of sheet metal bending process to predict the springback. *Materials and Design*, *31*(2), 657–662. https://doi.org/10.1016/j.matdes.2009.08.022.

Petru, C.-D., Crenganiș, M., Breaz, R.-E., Racz, S.-G., Gîrjob, C.-E., & Drașovean, P. (2024). Development of a digital twin for the ABB IRB 1200 robot in sheet metal forming processes. *Procedia Computer Science*, *242*, 228–235. https://doi.org/10.1016/j.procs.2024.08.253.

Sedlmaier, A., Dietl, T., & Ferreira, P. (2017). Digitalization in roll forming manufacturing. *Journal of Physics: Conference Series*, *896*, 12–38. https://doi.org/10.1088/1742-6596/896/1/012038.

Womack, J. P., & Jones, D. T. (1997). Lean thinking – banish waste and create wealth in your corporation. *Journal of the Operational Research Society*, *48*(11), 1144–1150. https://doi.org/10.1057/palgrave.jors.2600967.